Submitted to ADVANCED MATERIALS

Fast-response photonic device based on organic crystals heterojunctions assembled into a vertical-yet-open asymmetric architecture

Lei Zhang,[1] Egon Pavlica,[2] Xiaolan Zhong,[1] Fabiola Liscio,[3] Songlin Li,[1] Gvido Bratina,[2] Emanuele Orgiu[1,4] and Paolo Samorì[1]**

[1] Dr. L. Zhang, Dr. X. L. Zhong, Dr. S. L. Li, Prof. E. Orgiu, Prof. P. Samorì
University of Strasbourg, CNRS, ISIS UMR 7006
8 allée Gaspard Monge, F-67000 Strasbourg, France
E-mail: samori@unistra.fr

[2] Dr. E. Pavlica, Prof. G. Bratina
Laboratory of Organic Matter Physics, University of Nova Gorica
Vipavska 11c, SI-5270 Ajdovščina, Slovenia

[3] Dr. F. Liscio
Istituto per la Microelettronica e Microsistemi (IMM), Consiglio Nazionale delle Ricerche, via Gobetti 101, 40129 Bologna, Italy

[4] Present address: Prof. E. Orgiu
Institut National de la Recherche Scientifique (INRS), EMT Center, 1650 Blvd. Lionel-Boulet, J3X 1S2 Varennes, Québec, Canada.
E-mail: emanuele.orgiu@emt.inrs.ca

Keywords: Nanostructured electrode, photovoltaics, photodetector, organic electronics, crystal semiconductors

The integration of organic crystals into photovoltaic devices represents a powerful strategy to investigate exciton and charge transport in ordered organic semiconductors,[1] and it represents a promising approach towards high-performance and cost-effective photoelectrical conversion on flexible substrates.[2] These photonic devices can take advantage of the outstanding characteristics of organic semiconductors such as their tunable optoelectronic properties via design at the molecular and supramolecular level, their large absorption coefficient, etc.[3] Furthermore, the high efficiency of charge and exciton transport in crystals provides organic semiconductors the potential to rival amorphous silicon (α-Si).[4] For example, the exciton diffusion length in rubrene crystals could reach a few micrometers, being even comparable to the light absorption length.[5] Further, in some highly crystalline organic semiconductors, singlet fission was observed.[6] Such evidence suggests that organic crystals could be exploited in high performance photovoltaic devices to simultaneously achieve sufficient photon absorption and efficient exciton separation after rational interface engineering.[7,8]

However, structurally anisotropic self-assembled architectures such as organic crystals heterojunctions, whose shape and size can largely vary, are notoriously difficult to be integrated into the standard vertical geometry photovoltaic devices by making use of simple approaches.[9] Hitherto, planar devices with electrodes arranged in lateral configuration have been proved to be a feasible platform to demonstrate crystal-based organic photovoltaics.[10] Unfortunately, the long electrode-to-electrode distance (tens to hundreds micrometers) in such a geometry determines a slow photoresponse and significant charge recombination because the photo-generated charge carriers have to travel a long way before reaching the electrodes. In addition, extra effort is required to implement electrode asymmetry, i.e. having architectures with cathode and anode electrodes featuring different work-functions. Such asymmetry is vital to achieve a full control over the injection and extraction of either holes or electrons. Consequently, these limitations and challenges associated with device fabrication

make organic crystal-based photovoltaics less appealing in spite of its huge technological potential.

By taking advantage of a recently reported nanomesh scaffold, [11] herein we have successfully addressed this challenge by proposing a general strategy to simultaneously connect multiple nanowire/microplate crystals heterojunctions with honeycomb-shaped asymmetric nanoelectrodes (i.e., nanomesh scaffold) to explore their photovoltaic properties. By mastering a method which relies on phase transfer (PT), we have self-assembled N,N′-Dioctyl-3,4,9,10-perylenedicarboximide (PTCDI-C8) n-type crystalline nanowires (CNWs) as model system to demonstrate our device design.[12] Differently from the solvent-induced precipitation (SIP) nanowires integrated previously in the hollow-structured nanomesh scaffold,[11] here the greater crystalline nature and rigidity of PT-CNWs enables their integration in the nanomesh through the formation of a physical contact specifically only with the upper electrode while forming an air gap with the bottom electrode. Such air gap can be filled with a second semiconductor of opposite polarity (in this case p-type) in order to realize a p-n heterojunction by solution processing. We chose 6,13-Bis(triisopropylsilylethynyl) pentacene (TIPS-PEN), which exhibits high tendency to crystallize in solution, to be coupled to PTCDI-C8 because these two components exhibit complementary absorbance and therefore the device response can occur on a broader spectral region. In contrast to the conventional vertical diode architecture, where the semiconductor is sandwiched between the electrodes, our strategy adopts a vertical-yet-open device structure, which allows the successive deposition of each semiconductor after completion of electrodes patterning and possible interface engineering. Hence this method is versatile and can be exploited to integrate also other discrete organic crystalline semiconducting architectures into high performance optoelectronic devices in absence of transparent electrodes like ITO.

The fabrication steps of the nanomesh scaffold was monitored by scanning electron microscope (SEM) as shown in Figure S1. While we have already recently reported on the

fabrication of this nanomesh scaffold,[11] the major difference between the present work and our former publication relies on the rigidity of nanowire being integrated. In our previous work, highly conformal nanowires were employed at expenses of a not optimal degree of crystallinity. In the present paper we further extend the use of nanomesh scaffold to bi-crystalline structures for enhanced photonics response. PTCDI-C8 was chosen as a model system for these two contributions because of its propensity to stack forming one-dimensional nanowires with crystallinity and rigidity that can be tuned by the employed growth method, e.g. solvent induced precipitation (SIP) and phase transfer (PT) (Figure S2).[11,13] Generally, when the rate of the self-assembly process of PTCDI-C8 molecules is reduced, nanowires featuring higher crystalline degree, larger size and higher stiffness are produced.[14] For example, PT-CNWs are thicker (ca. 200 nm) and so more rigid than SIP-NWs, the latter exhibiting a typical thickness of 40-50 nm (Figure S3). As a result, when both these nanowires are deposited onto nanomesh scaffold, SIP-NWs are conformal enough to bend and to make electrical contact with both electrodes on the same time,[11] whereas PT-CNWs would be suspended across the nanoholes as shown in **Figure 1a** and **1b**. As we described above, the formation of air gap allows us to interface p- and n-type semiconductors with cathode and anode separately by filling the air-gap with the second semiconductor (Figure 1c).

Before spin-coating TIPS-PEN onto the nanomesh scaffold which has been decorated with PTCDI-C8 PT-CNWs, a thin layer of lithium fluoride (LiF) dielectric film is evaporated as the protecting layer (Figure 1c). In this way the TIPS-PEN makes electrical contact only with the masked area below the nanowire, in between the latter and the silicon electrode. This is because the whole surface has been passivated by LiF, except in the region of silicon electrode beneath nanowires, that act as shadowing mask for the deposition (Figure S4). Furthermore, LiF protecting shell could also improve the stability of PTCDI-C8 nanowires against solvent corrosion when TIPS-PEN/anisole solution is spin-coated (Figure S5, S6 and

S7). The solubility of PTCDI-C8 in anisole was also studied by UV-visible absorption spectroscopy (see Figure S8).

The optical microscopy (OM) and SEM images in Figure 1d and 1e portray the device surface being decorated with PTCDI nanowires and elongated TIPS-PEN microplates from top view and bird's-eye view, respectively. The appearance of birefringence, as evidenced by linearly-polarized microscopy images in Figure 1d, suggests the bi-crystal nature of PTCDI-C8 and TIPS-PEN which are both grown in solution.[12,15] The SEM image in Figure 1e shows the device morphology, formed by nanowires that are surrounded by microplates. It is evident that neither PTCDI-C8 nor TIPS-PEN can fully cover the surface, being a limit in the integral photocurrent for a given device surface area. Here we should note that the calibration of real p-n interface area, which is necessary to calculate the external quantum efficiency, becomes difficult because this interface is hidden under the PTCDI-C8 nanowires.[11]

XRD characterization casts light onto the molecular packing in the device. **Figure 2**a shows that SIP-derived nanowires are in the same crystallographic phase with nanowires grown through phase transfer. Thanks to the prolonged time for molecules to assemble during phase transfer, PT-CNWs exhibit much higher degree of crystallinity than SIP-NWs (Figure S2). All the XRD peaks measured on the final device (Figure 2b) could be unambiguously assigned to either PTCDI-C8 or TIPS-PEN crystals.[12,15] These distinct and intense XRD peaks, together with the birefringence (Figure 1d), provide unequivocal evidence for the high degree of order within the crystals as a prerequisite towards the fabrication of high performing crystals-based organic photovoltaic devices. Importantly, the two selected semiconductors, i.e. PTCDI-C8 and TIPS-PEN, exhibit complementary spectral features as evidenced by UV-visible absorption spectroscopy in Figure 2c. Hence photonic devices using these two molecules as absorbers should exhibit a broader wavelength coverage for the light energy exploitation. Here we should note TIPS-PEN and PTCDI-C8 could form exciton dissociation

favorable donor-acceptor-interface thanks to the properly aligned HOMO-LUMO energy levels. As shown in the inset of Figure 2c, both ΔLUMO (TIPS-PEN −3.4 eV *vs.* PTCDI-C8 −3.7 eV) and ΔHOMO (TIPS-PEN −5.1 eV *vs.* PTCDI-C8 −5.9 eV) are energetically large enough to drive interfacial charge transfer upon illumination.[11,15]

The *I-V* curves of the obtained optoelectronic device, recorded while irradiating with red, green, yellow and blue light are plotted in **Figure 3**a together with dark current. The signal-to-noise ratio always exceeds 10^7 under a bias of 0 V for monochromatic illumination. Under a 1.5 V bias voltage, the signal-to-noise ratio could still reach 10^4. The photovoltaic detector also exhibits outstanding current switching upon irradiation without appreciable relaxation and trailing (Figure 3a inset; Figure S9).[16] To clarify the origin of photocurrent in the crystal heterojunction, we recorded the short circuit current (I_{SC}) by changing the irradiation wavelength from 320 nm to 690 nm. Since the light power density upon wavelength is also uneven, we multiply UV-visible absorbance of each material with the spectral power density function of our light source to get two dashed lines shown in Figure 3b. Apparently, the photocurrent peaks could be ascribed to either PTCDI-C8 or TIPS-PEN, suggesting that both crystals have contributed to the overall photocurrent. We also compared the photoresponse of identical device before and after depositing TIPS-PEN (black line in Figure 3b and Figure S10), from which we can find the responsivity value dramatically increased of ca. 5000-folds upon TIPS-PEN deposition. The significant responsivity enhancement, together with the appearance of TIPS-PEN featured response peak at 640 nm, prove the successful fabrication of asymmetrical heterojunction.

In Figure 3c, we investigated the relationship between photocurrent and light intensity shone on the device. Because of the photocurrent saturation effect, the short circuit current would not increase linearly with more intensive illumination.[17] An external voltage bias or a built-in electrical field will be helpful to further improve the device performance by accelerating photo-generated charges towards the electrodes.[11] In the color-filling contour

image of Figure 3d, we also studied the open circuit voltage (V_{OC}) under different wavelength. The V_{OC} (ca. 0.35-0.40 V) is rather stable but slightly tuned by irradiation wavelength also. For the wavelength that TIPS-PEN exhibits more significant absorbance than PTCDI-C8, the device will show a relatively higher V_{OC}. This phenomenon might originate from the fact that ΔLUMO is smaller than ΔHOMO (0.3 eV vs. 0.8 eV) in the crystals heterojunction, so the excitons generated in TIPS-PEN will lose less energy when separated at p-n interface.[8] In Figure 3e and f, we illustrated the photo responsivity would be enhanced by applying a working voltage. For example, the responsivity has increased from 2.0 mA/W to 10 mA/W by applying a 1.5 V bias. For a given voltage bias, the photodetector will show a better responsivity under a lower incident light power. In fact, we have observed distinct wavelength-dependent photo responsivity even at ultralow light power density of 4-10 nW/cm^2 (see Figure S12), with the responsivity value being two-times larger than that taken under more intensive illumination shown in Figure 3f.

The short distances the dissociated excitons have to travel to reach electrodes in our geometry are supposed to result in a fast device photoresponse.[18] As shown in **Figure 4**a, we performed transient photo response characterization by irradiating the device with a 3-ns laser pulse (λ tunable in the range from 440 nm to 700 nm) and then recorded the photocurrent by an oscilloscope. The response time, i.e. the time needed for the photocurrent to peak, was always shorter than 100 ns with slight variations upon laser irradiation, especially for red light at λ = 700 nm, which is at the maximum absorption in TIPS-PEN, but where the absorption in PTCDI-C8 is lower. Therefore, we chose λ = 500 nm (absorption peak for PTCDI-C8 but valley for TIPS-PEN) together with λ = 700 nm as test wavelengths to investigate how the working voltage affects the device response time (Figure 4b). In accordance with Figure 4a, the 0 V photocurrent reaches its maximum in less time if the samples are illuminated by λ = 500 nm than with λ = 700 nm. In both irradiation wavelengths, the response time is further

improved, i.e., from 34 to 17 ns (λ = 500 nm) and from 93 to 36 ns (λ = 700 nm) by applying an external voltage of 1.5 V.

Thanks to the fast response, we demonstrated an interesting application for this high-speed photodetector. As shown in Figure 4c, we recorded very sharp peaks by scanning the monochromatic light wavelength between 300 nm and 690 nm rapidly. Zooming-up the peak into 1 ms timescale, we found that the profile, position and height of the photocurrent peaks were in perfect agreement with photocurrent spectrum taken on an identical device with much slower scanning speed of tens seconds (Figure 4d; dash line). This phenomenon strongly suggests that our crystal-based photodetector is able to record fast wavelength scanning within 1 ms with appreciable accuracy. More supporting experiments are provided in Figure S13 and S14. Here we note that the main limitation for higher time resolution is the large sampling intervals (ca. 0.2 ms) of the ammeter used.

This honeycomb-shaped device geometry also provides the possibility to tune the response spectrum by mixing different kinds of nanowires into a single optoelectronic device. In addition, other types of self-assembled nanofibers featuring tunable photoresponse and electrical properties can be envisaged by using this strategy.[19] Because the UV-visible absorbance is also dependent on the molecular aggregation state for a given material, here we demonstrated to blend PTCDI-C8 PT-CNWs and SIP-NWs with different ratio to tune the responsivity spectrum. As shown in Figure 4e, the location and intensity distribution of PT-CNWs and SIP-NWs absorption peaks are different, where the red shift of resonance peaks could be correlated to the increased crystalline degree. By mixing these two kinds of PTCDI-C8 nanowires together, we have developed photonic devices with tunable photoresponse spectra as determined by the UV-visible absorption (Figure 4f). Such result is very interesting because the response spectrum is tuned simply by molecular aggregation without influencing the HOMO-LUMO energy alignment in the system. In addition, the two electrodes can be functionalized by using either thiol- or silane/silazane chemistry, respectively for the top and

the bottom electrode. This allows to tune rather finely the wettability and work function of the electrodes and to maximize the energetic asymmetry which favors photon harvesting.[20]

In summary, we have reported a novel photovoltaic detector based on organic crystal heterojunction, and demonstrated its advantages including the ultrahigh signal-to-noise ratio of 10^7, ultrafast photoresponse less than 100 ns, tunable optoelectronic response spectrum and high sensitivity to light, even at low irradiation power. Our results prove that nanomesh scaffold is a powerful device platform to realize photoelectrical conversion in organic semiconducting nanowires regardless of their conformity. In principle, our approach is also applicable to all combinations of p-n organic semiconductors as long as they are processed using orthogonal solvents. In the future, many different kinds of organic crystalline nanowires with high absorption coefficient, long exciton diffusion length, the possibility to be processed in orthogonal solvents, as well as other desirable properties like singlet fission could also be incorporated into photovoltaic devices by the aid of nanomesh scaffold to make full use of their outstanding optoelectronic properties. Furthermore, ongoing study is undertaken to make our vertical-yet-open asymmetric architecture more general for the other discrete organic crystals of different shape and size besides phase transfer and solvent induced precipitation derived nanowires.

Experimental Section

Materials: Polystyrene (PS) nanospheres mono-dispersed suspension (10 w%, in water), lithium fluoride (99.995%), *N*,*N*′-Dioctyl-3,4,9,10-perylenedicarboximide (PTCDI-C8) (98%), and 6,13-Bis(triisopropylsilylethynyl)pentacene (TIPS-PEN) (>99%) were purchased from Sigma-Aldrich without further purification. The silicon wafer was purchased from IPMS

Fraunhofer (Dresden) with 90-nm thick SiO_2 layer grown by thermal oxidation (*n*-doping level ~3 10^{17} cm^{-3}).

Optoelectronic measurement: The optoelectronic characterization was performed in the glovebox filled with nitrogen. We used Polychrome V system as monochromatic light source, which was purchased from Till Photonics. The output power has been calibrated by PM100A Power Meter from Thorlabs company. Keithley 2636A system sourcemeter was used to make the electrical characterization.

Transient photoresponse characterization: The laser pulse duration was 3 ns, and its repetition rate was 10 Hz. All measurements were performed in a nitrogen atmosphere with H_20 and O_2 levels below 10 ppm. The Si substrate was referred as an anode and was connected to zero potential during the measurement. The AC signal from the cathode, separated by a circuit comprising a capacitor and a coil (bias-T) was connected to a 2 GHz current amplifier.

Supporting Information

Supporting Information is available online from the Wiley Online Library or from the author.

Acknowledgements

The technical help of the STnano cleanroom facility is gratefully acknowledged. This work was financially supported by EC through the ERC project SUPRAFUNCTION (GA-257305) and the Marie Curie ITN project iSwitch (GA No. 642196), the ANR Equipex Union (ANR-10-EQPX-52-01), the Labex projects CSC (ANR-10-LABX-0026 CSC) and NIE (ANR-11-LABX-0058 NIE) within the Investissement d'Avenir program ANR-10-IDEX-0002-02, and the International Center for Frontier Research in Chemistry (icFRC), and by the Slovenian Research Agency, program P1-0055.

Received: ((will be filled in by the editorial staff))

Revised: ((will be filled in by the editorial staff))

Published online: ((will be filled in by the editorial staff))

[1] a) I. N. Hulea, S. Fratini, H. Xie, C. L. Mulder, N. N. Iossad, G. Rastelli, S. Ciuchi, A. F. Morpurgo, *Nat. Mater.* **2006**, *5*, 982; b) H. Alves, A. S. Molinari, H. X. Xie, A. F. Morpurgo, *Nat. Mater.* **2008**, *7*, 574; c) R. M. Pinto, E. M. S. Macoas, A. I. S. Neves, S. Raja, C. Baleizao, I. C. Santos, H. Alves, *J. Am. Chem. Soc.* **2015**, *137*, 7104; d) J. Liu, H. Zhang, H. Dong, L. Meng, L. Jiang, L. Jiang, Y. Wang, J. Yu, Y. Sun, W. Hu, A. J. Heeger, *Nat. Commun.* **2015**, *6*, 10032; e) G. M. Akselrod, P. B. Deotare, N. J. Thompson, J. Lee, W. A. Tisdale, M. A. Baldo, V. M. Menon, V. Bulovic, *Nat. Commun.* **2014**, *5*, 3646; f) P. Irkhin, I. Biaggio, *Phys. Rev. Lett.* **2011**, *107*, 017402.

[2] a) H. Y. Li, C. C. Fan, W. F. Fu, H. L. L. Xin, H. Z. Chen, *Angew. Chem. Int. Ed.* **2015**, *54*, 956; b) S. M. Menke, W. A. Luhman, R. J. Holmes, *Nat. Mater.* **2013**, *12*, 152; c) Z. M. Beiley, M. G. Christoforo, P. Gratia, A. R. Bowring, P. Eberspacher, G. Y. Margulis, C. Cabanetos, P. M. Beaujuge, A. Salleo, M. D. McGehee, *Adv. Mater.* **2013**, *25*, 7020.

[3] a) M. S. Vezie, S. Few, I. Meager, G. Pieridou, B. Dorling, R. S. Ashraf, A. R. Goni, H. Bronstein, I. McCulloch, S. C. Hayes, M. Campoy-Quiles, J. Nelson, *Nat. Mater.* **2016**, *15*, 746; b) A. Liess, M. Stolte, T. He, F. Würthner, *Mater. Horizons* **2016**, *3*, 72; c) W. Zhu, R. Zheng, Y. Zhen, Z. Yu, H. Dong, H. Fu, Q. Shi, W. Hu, *J. Am. Chem. Soc.* **2015**, *137*, 11038; d) H. T. Yi, M. M. Payne, J. E. Anthony, V. Podzorov, *Nat. Commun.* **2012**, *3*, 1259; e) C. L. Wang, H. L. Dong, W. P. Hu, Y. Q. Liu, D. B. Zhu, *Chem. Rev.* **2012**, *112*, 2208; f) M. Gsanger, J. H. Oh, M. Konemann, H. W. Hoffken, A. M. Krause, Z. N. Bao, F. Würthner, *Angew. Chem. Int. Ed.* **2010**, *49*, 740; g) A. C. Arias, J. D. MacKenzie, I. McCulloch, J. Rivnay, A. Salleo, *Chem. Rev.* **2010**, *110*, 3.

[4] a) K. Kim, Y. Rho, Y. Kim, S. H. Kim, S. G. Hahm, C. E. Park, *Adv. Mater.* **2016**, *28*, 3209; b) Y. Krupskaya, M. Gibertini, N. Marzari, A. F. Morpurgo, *Adv. Mater.* **2015**, *27*, 2453; c) A. Ciavatti, E. Capria, A. Fraleoni-Morgera, G. Tromba, D. Dreossi, P. J. Sellin, P. Cosseddu, A. Bonfiglio, B. Fraboni, *Adv. Mater.* **2015**, *27*, 7213; d) T. He, M. Stolte, F. Würthner, *Adv. Mater.* **2013**, *25*, 6951; e) H. Minemawari, T. Yamada, H. Matsui, J. Tsutsumi, S. Haas, R. Chiba, R. Kumai, T. Hasegawa, *Nature* **2011**, *475*, 364; f) R. R. Lunt, J. B. Benziger, S. R. Forrest, *Adv. Mater.* **2010**, *22*, 1233; g) R. J. Li, W. P. Hu, Y. Q. Liu, D. B. Zhu, *Acc. Chem. Res.* **2010**, *43*, 529; h) A. S. Molinari, H. Alves, Z. Chen, A. Facchetti, A. F. Morpurgo, *J. Am. Chem. Soc.* **2009**, *131*, 2462; i) J. Roncali, P. Leriche, A. Cravino, *Adv. Mater.* **2007**, *19*, 2045.

[5] H. Najafov, B. Lee, Q. Zhou, L. C. Feldman, V. Podzorov, *Nat. Mater.* **2010**, *9*, 938.

[6] a) D. N. Congreve, J. Y. Lee, N. J. Thompson, E. Hontz, S. R. Yost, P. D. Reusswig, M. E. Bahlke, S. Reineke, T. Van Voorhis, M. A. Baldo, *Science* **2013**, *340*, 334; b) W. L. Chan, M. Ligges, A. Jailaubekov, L. Kaake, L. Miaja-Avila, X. Y. Zhu, *Science* **2011**, *334*, 1541; c) M. B. Smith, J. Michl, *Chem. Rev.* **2010**, *110*, 6891.

[7] a) K. Vandewal, J. Widmer, T. Heumueller, C. J. Brabec, M. D. McGehee, K. Leo, M. Riede, A. Salleo, *Adv. Mater.* **2014**, *26*, 3839; b) K. Vandewal, S. Albrecht, E. T. Hoke, K. R. Graham, J. Widmer, J. D. Douglas, M. Schubert, W. R. Mateker, J. T. Bloking, G. F. Burkhard, A. Sellinger, J. M. J. Fréchet, A. Amassian, M. K. Riede, M. D. McGehee, D. Neher, A. Salleo, *Nat. Mater.* **2014**, *13*, 63; c) A. Tada, Y. F. Geng, Q. S. Wei, K. Hashimoto, K. Tajima, *Nat. Mater.* **2011**, *10*, 450.

[8] W. J. Potscavage, A. Sharma, B. Kippelen, *Acc. Chem. Res.* **2009**, *42*, 1758.

[9] a) K. S. Park, K. S. Lee, C. M. Kang, J. Baek, K. S. Han, C. Lee, Y. E. K. Lee, Y. Kang, M. M. Sung, *Nano Lett.* **2015**, *15*, 289; b) Y. L. Lei, L. S. Liao, S. T. Lee, *J. Am. Chem. Soc.* **2013**, *135*, 3744; c) I. G. Lezama, M. Nakano, N. A. Minder, Z. H. Chen, F. V. Di Girolamo, A. Facchetti, A. F. Morpurgo, *Nat. Mater.* **2012**, *11*, 788.

[10] a) M. Kim, J. H. Park, J. H. Kim, J. H. Sung, S. B. Jo, M. H. Jo, K. Cho, *Adv. Energy Mater.* **2015**, *5*, 1401317; b) Q. H. Cui, L. Jiang, C. Zhang, Y. S. Zhao, W. P. Hu, J. N. Yao, *Adv. Mater.* **2012**, *24*, 2332; c) Y. J. Zhang, H. L. Dong, Q. X. Tang, S. Ferdous, F. Liu, S. C. B. Mannsfeld, W. P. Hu, A. L. Briseno, *J. Am. Chem. Soc.* **2010**, *132*, 11580.

[11] L. Zhang, X. Zhong, E. Pavlica, S. Li, A. Klekachev, G. Bratina, T. W. Ebbesen, E. Orgiu, P. Samorì, *Nat. Nanotech.* **2016**, *11,* 900.

[12] A. L. Briseno, S. C. B. Mannsfeld, C. Reese, J. M. Hancock, Y. Xiong, S. A. Jenekhe, Z. Bao, Y. N. Xia, *Nano Lett.* **2007**, *7*, 2847.

[13] a) L. Zang, Y. K. Che, J. S. Moore, *Acc. Chem. Res.* **2008**, *41*, 1596; b) K. Balakrishnan, A. Datar, R. Oitker, H. Chen, J. M. Zuo, L. Zang, *J. Am. Chem. Soc.* **2005**, *127*, 10496.

[14] a) J. F. Geng, W. Z. Zhou, P. Skelton, W. B. Yue, I. A. Kinloch, A. H. Windle, B. F. G. Johnson, *J. Am. Chem. Soc.* **2008**, *130*, 2527; b) Y. K. Che, A. Datar, K. Balakrishnan, L. Zang, *J. Am. Chem. Soc.* **2007**, *129*, 7234.

[15] a) S. Y. Cho, J. M. Ko, J. Y. Jung, J. Y. Lee, D. H. Choi, C. Lee, *Org. Electron.* **2012**, *13*, 1329; b) O. L. Griffith, J. E. Anthony, A. G. Jones, D. L. Lichtenberger, *J. Am. Chem. Soc.* **2010**, *132*, 580; c) R. Hamilton, J. Smith, S. Ogier, M. Heeney, J. E. Anthony, I. McCulloch, J. Veres, D. D. C. Bradley, T. D. Anthopoulos, *Adv. Mater.* **2009**, *21*, 1166; d) S. K. Park, T. N. Jackson, J. E. Anthony, D. A. Mourey, *Appl. Phys. Lett.* **2007**, *91*, 063514.

[16] a) P. Irkhin, H. Najafov, V. Podzorov, *Sci. Rep.* **2015**, *5*, 15323; b) O. Ostroverkhova, D. G. Cooke, F. A. Hegmann, J. E. Anthony, V. Podzorov, M. E. Gershenson, O. D. Jurchescu, T. T. M. Palstra, *Appl. Phys. Lett.* **2006**, *88*, 162101.

[17] a) A. K. K. Kyaw, D. H. Wang, V. Gupta, W. L. Leong, L. Ke, G. C. Bazan, A. J. Heeger, *ACS Nano* **2013**, *7*, 4569; b) S. R. Cowan, N. Banerji, W. L. Leong, A. J. Heeger, *Adv. Funct. Mater.* **2012**, *22*, 1116.

[18] K. J. Baeg, M. Binda, D. Natali, M. Caironi, Y. Y. Noh, *Adv. Mater.* **2013**, *25*, 4267.

[19] a) J. M. Mativetsky, E. Orgiu, I. Lieberwirth, W. Pisula, P. Samorì, *Adv. Mater.* **2014**, *26*, 430; b) R. C. Savage, E. Orgiu, J. M. Mativetsky, W. Pisula, T. Schnitzler, C. L. Eversloh, C. Li, K. Müllen, P. Samorì, *Nanoscale* **2012**, *4*, 2387; c) R. C. Savage, J. M. Mativetsky, E. Orgiu, M. Palma, G. Gbabode, Y. H. Geerts, P. Samorì, *J. Mater. Chem.* **2011**, *21*, 206; d) C. E. Finlayson, R. H. Friend, M. B. J. Otten, E. Schwartz, J. J. L. M. Cornelissen, R. J. M. Nolte, A. E. Rowan, P. Samorì, V. Palermo, A. Liscio, K. Peneva, K. Müllen, S. Trapani, D. Beljonne, *Adv. Funct. Mater.* **2008**, *18*, 3947.

[20] a) B. de Boer, A. Hadipour, M. M. Mandoc, T. van Woudenbergh, P. W. M. Blom, *Adv. Mater.* **2005**, *17*, 621; b) M. L. Sushko, A. L. Shluger, *Adv. Mater.* **2009**, *21*, 1111; c) C. Vericat, M. E. Vela, G. Benitez, P. Carro, R. C. Salvarezza, *Chem. Soc. Rev.* **2010**, *39*, 1805; d) K.-Y. Wu, S.-Y. Yu, Y.-T. Tao, *Langmuir* **2009**, *25*, 6232; e) S. Kobayashi, T. Nishikawa, T. Takenobu, S. Mori, T. Shimoda, T. Mitani, H. Shimotani, N. Yoshimoto, S. Ogawa, Y. Iwasa, *Nat. Mater.* **2004**, *3*, 317.

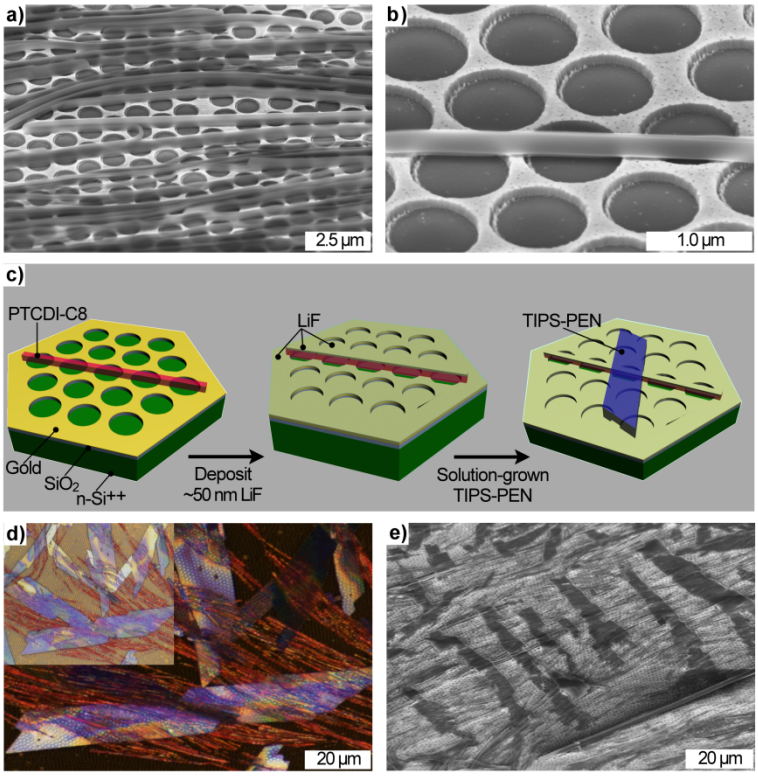

Figure 1. a) Phase-transfer derived PTCDI-C8 crystalline nanowires (PT-CNWs) on nanomesh electrode (Bird's-eye-view). b) The air gap between PT-CNWs and silicon electrode (substrates tilt by 54°). c) Schematic diagram illustrating the deposition sequence of PTCDI-C8 crystalline nanowires and TIPS-PEN microplates towards asymmetrical heterojunction on nanomesh scaffold. d) Birefringence of PTCDI-C8 (red) and TIPS-PEN (blue) as evidenced by (linearly-)polarized optical microscopy. Inset shows optical microscope image taken at the same position with a non-polarized light source. e) Bird's-eye-view of the device morphology taken by SEM (tilt by 54°).

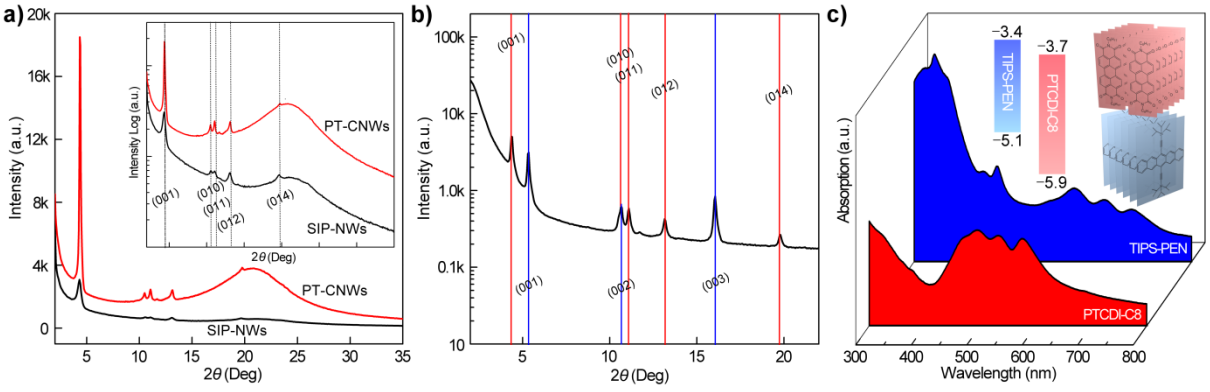

Figure 2. a) XRD characterization of PTCDI-C8 nanowires produced by different methods (red line, phase transfer; black line, solvent-induced-precipitation). b) XRD characterization of PTCDI-C8/TIPS-PEN bi-crystals device. Red lines indicate lattice planes for PTCDI-C8, meanwhile blue lines represent those from TIPS-PEN. c) UV-Visible absorbance of PTCDI-C8 PT-CNWs and TIPS-PEN crystals on quartz respectively. Inset shows the molecular structure and HOMO-LUMO energy level of both materials.

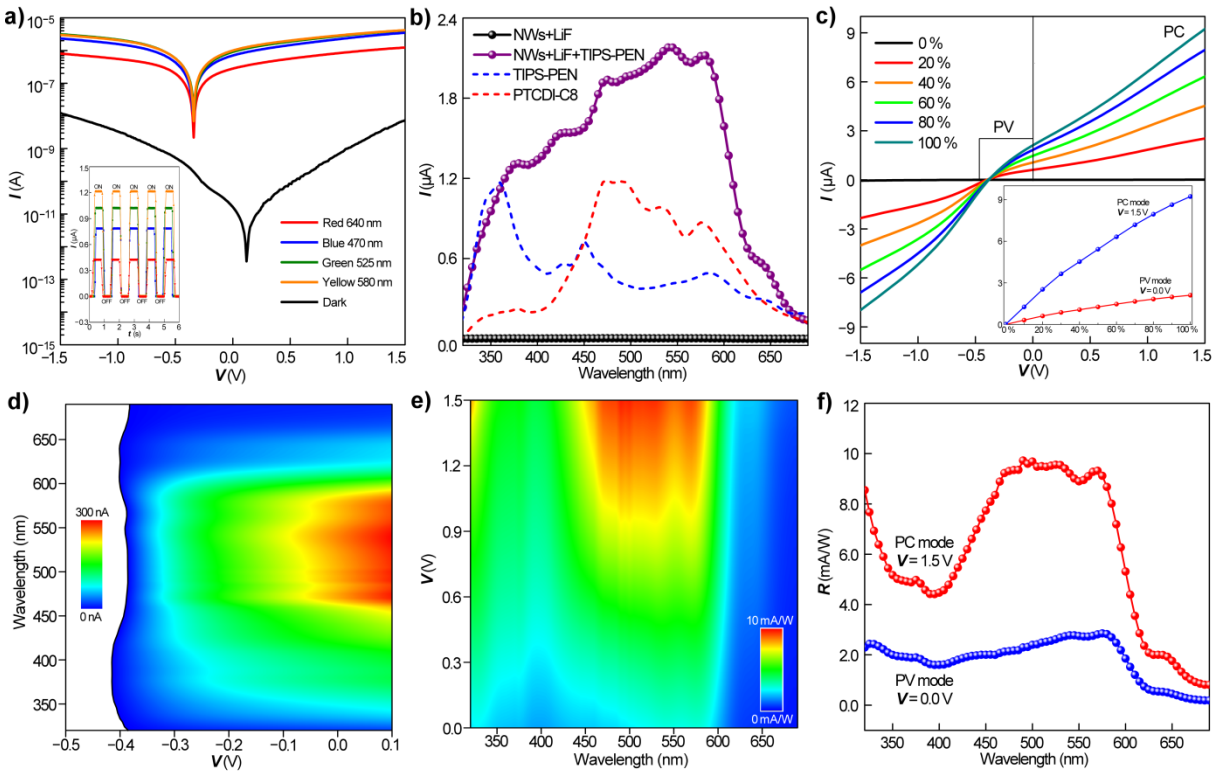

Figure 3. a) *I-V* curves under illumination conditions of dark state and four different colors with light power density unified to be ca. 2.9 mW/cm^2. Inset shows the optoelectrical switching behavior under 0 V bias and being irradiated with red, blue, green and yellow light. b) Short circuit current (I_{SC}) plotted by irradiation wavelength for both the bi-crystals photonic device (purple line) and the identical device before depositing TIPS-PEN (black line). The blue and red dash lines indicate the absorption spectra of nanowires and microplates respectively multiplied by the light power density spectra used here. c) *I-V* curves under varying light power intensity of 500 nm green light where 100% equals to 5.766 mW shone

on the device. Inset shows the relationship between photocurrent and light intensity under 0 V (PV represents photovoltaic) and 1.5 V (PC means photoconduction). d) The current recorded at different voltage and wavelength (–0.5 V to 0.1 V; 320 nm to 690 nm). Negative current has been set to white in order to visually emphasize the border of 2D contour image which represents V_{OC}. e) Color-filling contour image of photo responsivity (R) as a function of bias and wavelength. f) Photo responsivity in PC mode (1.5 V bias) and PV mode (0 V) extracted from Fig. 4e. Interestingly, the shape of responsivity spectrum could be tuned by applying different voltage. Upon this phenomenon, further experimental detail and discussion were supplied in Figure. S11.

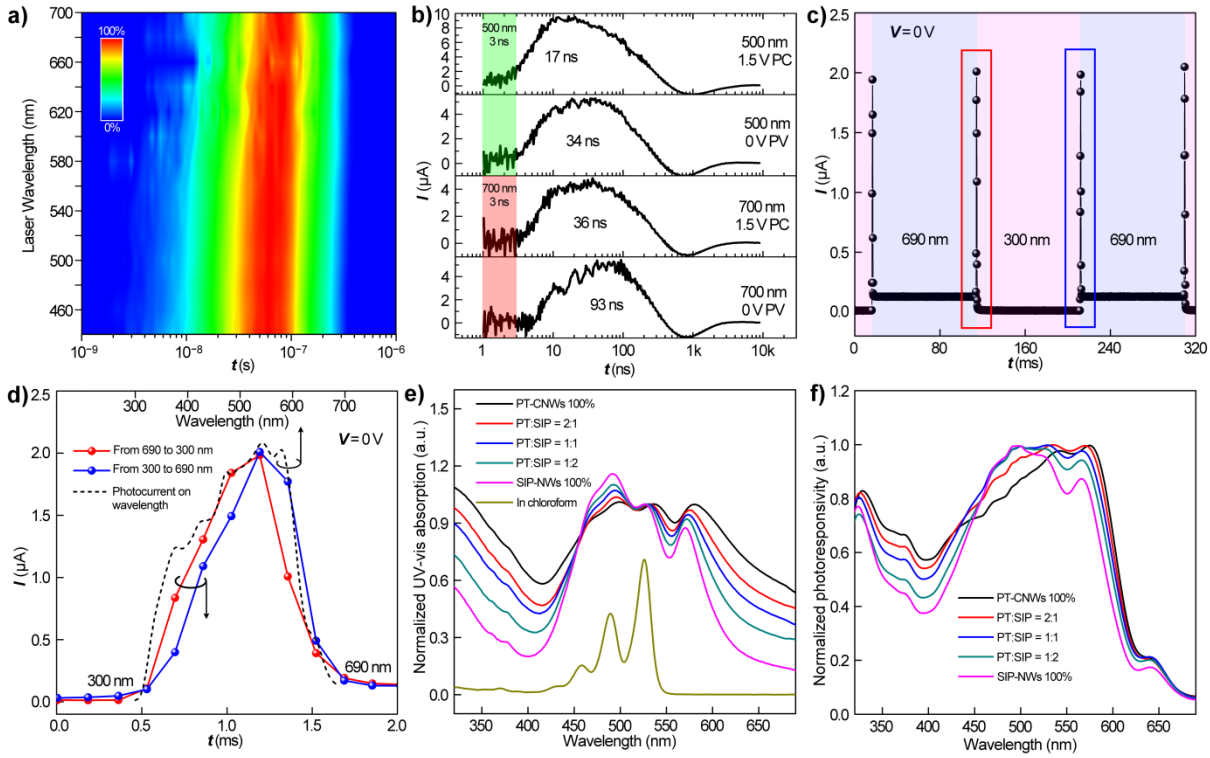

Figure 4. a) Transient photo response upon irradiation wavelength for PTCDI-C8 PT-CNWs and TIPS-PEN microplates system. b) Photocurrent as a function of time for the identical device in PC (1.5 V bias) and PV (0 V bias) modes respectively. Light with wavelength of 700 nm is used to selectively irradiate TIPS-PEN with minimized influence on PTCDI-C8 PT-CNWs according to the UV-vis absorption spectrum. c) Photocurrent recorded by rapidly

scanning irradiation wavelength from 300 nm to 690 nm and back repeatedly. d) Zoom into the rectangles in c) and comparison to photocurrent recorded by scanning irradiation wavelength from 300 to 690 slowly on an identical device. e) Normalized UV-visible absorption spectra of the mixture of nanowires produced by phase transfer and solvent induced precipitation with different ratio. f) Normalized photo responsivity spectra of the device made of mixed nanowires (PT-CNWs and SIP-NWs).